Journal of Hydrology 502 (2013) 202–211

Contents lists available at ScienceDirect

Journal of Hydrology

journal homepage: www.elsevier.com/locate/jhydrol

# Lacustrine groundwater discharge: Combined determination of volumes and spatial patterns

Karin Meinikmann *, Jörg Lewandowski, Gunnar Nützmann

*Leibniz-Institute of Freshwater Ecology and Inland Fisheries, Müggelseedamm 310, 12587 Berlin, Germany*

ARTICLE INFO

*Article history:*
Received 26 April 2013
Received in revised form 8 August 2013
Accepted 14 August 2013
Available online 22 August 2013
This manuscript was handled by Corrado Corradini, Editor-in-Chief, with the assistance of Aldo Fiori, Associate Editor

*Keywords:*
Groundwater–surface water interaction
Groundwater recharge
Lacustrine groundwater discharge
Water balance
Nutrient budget

SUMMARY

The quantification of lacustrine groundwater discharge (LGD) in water and nutrient balances of lakes is challenging and thus often neglected. However, by carrying large nutrient loads, groundwater might play a key role in a lakés nutrient budget even if its contribution to the water balance is small. In the present study, we quantify the total annual LGD of a lake in northeastern Germany by the calculation of annual groundwater recharge in the subsurface catchment. Furthermore, spatial variability of LGD is expected to have significant influence on the nutrient balance due to heterogeneous nutrient concentrations. To assess its spatial variability, LGD is calculated for single sites based on vertical temperature profiles of the lake bed along the shoreline. The combination of the total LGD and the spatial LGD patterns allows calculating LGD volumes for single shoreline sub-sections. These calculations reveal that a large portion of the total LGD enters the lake within a relatively limited section of the shoreline. Scenarios including different phosphorus concentrations demonstrate the importance of both, quantity and patterns of LGD, when groundwater-borne phosphorus loads are calculated. At high, heterogeneous groundwater nutrient concentrations, it is crucial for lake nutrient budgets to reliably determine LGD patterns and volume.



## 1. Introduction

Research on groundwater–surface water interactions focused mainly on streams and rivers in the past decades (Kalbus et al., 2006; Stonestrom and Constantz, 2003). Although there have been some early studies on lake interactions with groundwater (e.g. Meyboom, 1967, and a review by Winter, 1999) lake ecosystems were far less intensely investigated. This may be attributable to the fact that lakes had already been recognized as integrated systems in limnology for a long time while hydrologists and stream ecologists had predominantly been focusing on stream-specific topics (Moss, 2012). A revision of this one-dimensional view on river ecosystems might have led to the intense focus on the interactions of streams and groundwater, rather than of lakes and groundwater.

Furthermore, a general underestimation of the influence of groundwater on the omnipresent phenomenon of lake eutrophication might have led to a strong focus on in-lake processes and above-ground nutrient inputs. In this context, point sources of nutrients were identified as major threats for surface waters. In Europe, great effort was undertaken to reduce these point sources during the last decades. However, a "good chemical and ecological status" as being demanded by the European Water Framework Directive is still not established in many European freshwaters. After a significant reduction of point sources it becomes more and more obvious that the diffuse transport of nutrients into lakes limits their ecological regeneration to a larger extent than previously expected. Gelbrecht et al. (2005) attributed this to an ongoing nutrient leaching from agricultural areas on the one hand, and to the degradation of natural retention areas on the other hand. Widely discussed is also the contamination of groundwater by domestic wastewater exfiltration from faulty sewers and septic systems (Bremer and Harter, 2012; Katz et al., 2011; Ptacek, 1998; Robertson, 2008). Apart from the causes of groundwater contamination, the quantification of resulting nutrient loads to lakes is difficult and still lacking practical approaches. As a consequence, the groundwater path is often disregarded which might lead to a severe underestimation of its impact on the trophic state of a lake.

In the case of Lake Arendsee in northeastern Germany the groundwater path was also disregarded as a source of eutrophication. During the last four decades an increase of total phosphorus (TP) concentrations in the lake water from 0.15 to currently 0.19 mg $l^{-1}$ has been observed. As a result, severe blooms of cyanobacteria occurred periodically, which have stimulated discussion and request of lake restoration measures. While investigating different phosphorus (P) sources, we detected high (>1 mg $l^{-1}$) concentrations of soluble reactive phosphorus (SRP) in some parts

* Corresponding author. Tel.: +49 3064181671.
*E-mail address:* meinikmann@igb-berlin.de (K. Meinikmann).

0022-1694/$ - see front matter © 2013 Elsevier B.V. All rights reserved.
http://dx.doi.org/10.1016/j.jhydrol.2013.08.021

of the near-shore groundwater. Accordingly, we hypothesized that groundwater-borne nutrients, especially P, have a significant impact on the nutrient budget of the lake.

To reliably quantify the groundwater component in the P budget of the lake, an approach is required that considers both spatial variations of P concentrations and spatial heterogeneities in lacustrine groundwater discharge (LGD). These heterogeneities are introduced by small- to medium-scale variability of the aquifer characteristics, which in most cases are neither homogeneous nor isotropic (Rosenberry and LaBaugh, 2008). To address both, LGD quantity and quality, the approach needs to incorporate total LGD volumes as well as spatial LGD patterns. Thus, we combine a method of point measurements to detect LGD patterns with an integrating approach for total groundwater recharge quantification. In particular, we hypothesize that LGD into Lake Arendsee underlies a variety of small- to medium-scale geologic and anthropogenic impacts resulting in a large variability of LGD patterns along the shoreline. We furthermore hypothesize that hydraulic head contour lines (as a prerequisite for further investigations) do not depict this heterogeneity adequately due to an insufficient number of groundwater observation wells. Moreover, a large hydraulic gradient might indicate intense groundwater exfiltration, but can also be a consequence of low hydraulic conductivity ($k_{sat}$). Additionally, even an aquifer with a high $k_{sat}$ can result in little exfiltration in case that its thickness is small.

In recent years, using heat as a natural tracer has become more and more popular in research addressing small- to medium-scale interactions between groundwater and streams (Anderson, 2005; Constantz, 2008; Stonestrom and Constantz, 2003). We thus assume a great benefit by applying such a method also to groundwater–lake interfaces. Vertical temperature profiles in the sediment of surface waters are a function of advective and conductive heat exchange across the groundwater–surface water interface. Significant differences between temperatures of groundwater and surface water typically occur during summer and winter seasons. Therefore, the curvatures of temperature gradients in the sediment close to the interface represent the direction and intensity of vertical groundwater exchange. As described by Schmidt et al. (2006), a quantification of LGD rates from temperature profiles is possible using the heat transport equation to calculate the exchange rates. In the present study, temperature gradients of the lake sediment were used to determine spatial LGD patterns and intensity, rather than for calculation of absolute LGD.

Point measurements of LGD based on temperature depth profiles are combined with an integrating approach of groundwater recharge calculation for the whole catchment in order to derive LGD volumes for shoreline sub-sections. Based on a couple of near-shore groundwater wells P loads of three scenarios are calculated to evaluate the necessity of segmented approaches. With this study we demonstrate the importance of heterogeneities in LGD for the accuracy of groundwater-borne nutrient loads in lakes.

## 2. Methods

### 2.1. Study site

Lake Arendsee in north–northeastern Germany (Federal State of Saxony-Anhalt) is a deep stratified lake with a maximum depth of 50 m and a mean depth of about 30 m. A bathymetric map is provided in Hupfer and Lewandowski (2005). The lake covers an area of 5.1 km$^2$. Originally it was solely groundwater-fed and had no surface in- or outflows. Nowadays, there are four drainage ditches discharging to the lake. Three of them drain the subsurface catchment of the lake, while the fourth transports an additional amount of water from an adjacent watershed into the lake. Furthermore, an artificial outlet exists, where a weir regulates the outflow. The surface catchment (29.5 km$^2$ of size) is dominated by agricultural and forest land use, while the homonymous city of Arendsee is situated directly at the southern and south-western shoreline (Fig. 1A). Inclination is low in the surface catchment and thus, no significant surface runoff occurs.

For the subsurface catchment, previous (unpublished) studies agreed on a mainly northern groundwater flow direction resulting in LGD at the southern shoreline. However, size, shape, and hydraulic characteristics of the subsurface catchment were unknown. The setup of ten new groundwater observation wells at four sites along the southern shoreline (Fig. 1A) at the beginning of the present study revealed a variety of Pleistocene substrates. Values for $k_{sat}$ ranged from $0.33 \times 10^{-4}$ to $5.69 \times 10^{-4}$ m s$^{-1}$ in different depths from 3 to 34 m below surface, with maximum values at Sites 2 and 3 (Fig. 1A and B). Furthermore, the borehole profiles revealed that several near-surface aquifers exist that are hydrologically connected by geologic windows. The upper one, consisting of Saalian substrates, is separated from the aquifer below by Saalian or Holsteinian aquitards. South and south-east of the lake the lower aquifer originates mainly from Pleistocene sediments of the Saalian and Elstarian glacials. In western direction the deeper parts of the aquifer become dominated by Miocene substrates. However, the aquitard is not everywhere present, and thus, in some areas the sediments form a single aquifer. In some parts, the uppermost sediments consist of Pleistocene boulder clay formations with low $k_{sat}$, which also might have an influence on LGD intensities at the shoreline (Fig. 1B). Groundwater SRP concentrations at these four sites vary broadly between 0.08 and 1.21 mg SRP l$^{-1}$ with maximum concentrations at Site 3 in Fig. 1A and B.

### 2.2. Delineation of subsurface catchment

The size of the subsurface catchment is a necessary prerequisite to calculate groundwater recharge. We collected and evaluated available geological data to select appropriate groundwater observation wells and used 33 wells for the delineation of the subsurface catchment. Measurements were conducted at two consecutive days in July 2012. There was no rainfall during the campaign and a few days before. Thus, the measured groundwater heads can be assumed to be in a steady state.

Based on groundwater head data and the lake water level, hydraulic head contour lines were interpolated. All data were referred to sea level with the help of a tachymeter (Leica TSP 1200+). Measured groundwater head data were interpolated to contour lines by kriging using Surfer 8.0 (Golden Software©). Catchment boundaries were defined as the divide between groundwater flowing into the lake and groundwater flowing in other directions.

### 2.3. Mean annual groundwater recharge

According to the definition of a lake's catchment the mean total annual volume of LGD is equivalent to the mean total annual groundwater recharge in the whole catchment. Groundwater recharge can be quantified by a range of different approaches and methods have to be chosen carefully and on an individual basis (Scanlon et al., 2002). Due to the medium scale of the subsurface catchment, a method was chosen that calculates mean annual actual evapotranspiration $\overline{ETa}$ (l m$^{-2}$ yr$^{-1}$) as a factor controlling mean annual groundwater recharge. The approach by Glugla et al. (2003) is a refined method to calculate $\overline{ETa}$ based on the differential equation by Bagrov (1953):

$$\frac{d\overline{ETa}}{d\overline{P_{korr}}} = 1 - \left(\frac{\overline{ETa}}{\overline{ET\,\max}}\right)^n \quad (1)$$

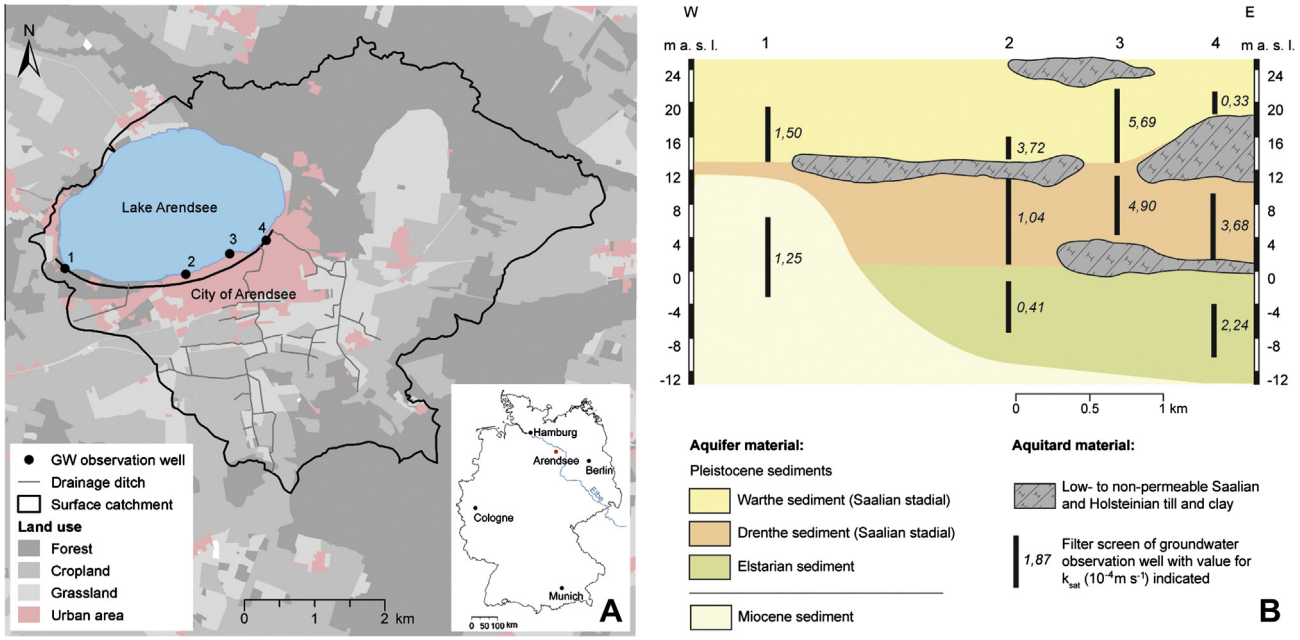


**Fig. 1.** Land use in the surface catchment and position of near-shore groundwater (GW) observation wells (A) and scheme of the geologic conditions along the southern shoreline of Lake Arendsee (B). The black line along the southern shoreline in A represents the cross-section in B. Mean concentrations of soluble reactive phosphorus (SRP, mg $l^{-1}$) observed in the different GW observation wells at each site are 0.09 (Site 1), 0.16 (Site 2), 1.21 (Site 3), and 0.08 (Site 4). Data are available from monthly or trimonthly measurements from April 2010 to December 2012, and means are weighted by the thicknesses of geologic layers in which the wells are located.

where $\overline{P_{korr}}$ (l $m^{-2}$ $yr^{-1}$) is the corrected mean annual precipitation, $\overline{ET\,\max}$ (mm $yr^{-1}$) is the mean maximum annual evapotranspiration, and $n$ is the parameter of effectiveness. $\overline{ET\,\max}$ is the result of a land use-dependent modification of the mean annual potential evapotranspiration $\overline{ETpot}$ (l $m^{-2}$ $yr^{-1}$) by a factor $f$. This modification is one of several aspects that had been advanced compared to the original method in order to represent land use and soil parameters that influence site-specific $\overline{ETpot}$. The method in general aims to determine $\overline{ETa}$ from its ratio to $\overline{ET\,\max}$. For a known $n$ this ratio can be derived from the graphical depiction of the Bagrov-Relation for any site of interest in Germany (Fig. 2). $n$ represents site conditions for the utilization of water and energy supply.

As a further advance of the method (Glugla et al., 2003), site-specific values for both, $n$ and $f$, can be determined by algorithms which base upon the evaluation of extensive lysimeter and climatic measurements in whole Germany and upon land use types. Six different land use types are covered by this method, namely sealed areas, areas without vegetation, grassland, cropland, deciduous forests and coniferous forests. Further data on specific field capacity and other specifications (e. g. population ages of forest stands and height of grassland vegetation) are required. Due to the availability of relevant soil data (especially specific field capacity) from a database of the Federal State of Saxony-Anhalt, the calculations were conducted at a higher spatial resolution than suggested by Glugla et al. (2003). Combinations of these data with land use data using ArcGIS 10.1 software (ESRI©) resulted in sub-areas for which groundwater recharge calculations were done individually. Due to a lack of this high resolution soil data for urban areas we used the soil survey map of the German Federal Institute for Geosciences and Natural Resources (BÜK 1000, 1998), which presents soil types at a lower resolution as originally suggested by Glugla et al. (2003). The predominant soil types defined three further sub-areas located in the area of the City of Arendsee. In these cases, values for specific field capacity as a prerequisite for the following calculations were chosen according to the recommendation of Glugla et al. (2003). Calculations were conducted for only 70% of the urban area, assuming a general portion of 30% being sealed and thus not contributing to groundwater recharge. Urban sub-areas were furthermore treated as grasslands, since it can be assumed that most of the unsealed area is covered with vegetation (e. g. lawns in public parks or private gardens).

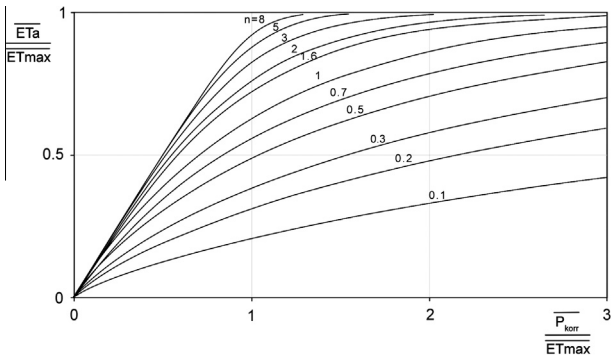


**Fig. 2.** Graphical scheme of the Bagrov-Relation (Eq. (1)) including corrected mean annual precipitation ($\overline{P_{korr}}$) and mean maximum annual evapotranspiration ($\overline{ET\,\max}$) as well as the parameter of effectiveness $n$ (modified from Glugla et al., 2003).

Values for $n$ were employed to derive the ratio of $\overline{ETa}$ to $\overline{ET\,\max}$ for the sub-areas arising from intersections of soil and land use data (Fig. 2). Resulting $\overline{ETa}$ is subtracted from $\overline{P_{korr}}$ to derive the total discharge $\overline{R}$ (l $m^{-2}$ $yr^{-1}$):

$$\overline{R} = \overline{P_{korr}} - \overline{ETa} \quad (2)$$

Since inclination is not relevant in the catchment of the lake, surface and lateral runoff were set to zero and groundwater recharge equals $\overline{R}$. However, for crop- and grasslands, drainage water extractions had to be considered. In general, such data are rarely existent but in the present case study they were available as drainage intensities. Four drainage intensity classes were assigned to single sub-areas of the catchment (0–30, 30–60, 60–90, and 90–100% drainage intensity). They were combined with the aforementioned data using ArcGIS 10.1 (ESRI©) to finally generate groundwater recharge rates and volumes for each sub-area. To

distinguish the results of these drainage calculations from actual drainage measurements (see Section 2.4) we call them "calculated drainage".

### 2.4. Measured drainage water extraction in the subsurface catchment

A validation of groundwater recharge calculation was performed using a dataset of a one-year-period of high resolution measurements of discharge in the aforementioned drainage ditches. The measurement equipment was mainly established for the quantification of P loads from agricultural drainage discharging into Lake Arendsee. Three of four drainage ditches contribute to discharge generated in the subsurface catchment of Lake Arendsee (Fig. 1A). The fourth ditch is situated outside of the subsurface catchment of the lake and is thus not relevant in the present context. Measurements were conducted close to the outlets into the lake. In one case, discharge was measured in 10 min-intervals by an ultrasonic flow measurement device. The other two ditches were equipped with V-weirs and pressure sensors to record water levels discharge and thus discharge in 30 min-intervals. The measurement period was from beginning of August 2010 until the end of July 2011.

### 2.5. Identification of LGD patterns using vertical lake bed temperature profiles

Lake bed temperature profiles at Lake Arendsee were measured approximately every 200 m along the southern part of the lake shoreline, where according to the delineation of the catchment LGD was expected to take place. LGD is known to primarily occur close the shore (Kishel and Gerla, 2002) and to decrease at least for homogeneous sediments with increasing distance to the shoreline (McBride and Pfannkuch, 1975). Based on this we focused our studies on the shoreline of the lake. Four vertical temperature profiles were obtained at each of 26 observation sites, arranged in transects of increasing distance to the shoreline (0.5 m, 1 m, 2 m, and 4 m, respectively). We used a stainless steel multilevel temperature probe including 16 equidistant thermistors of the type NTC 10 K (TDK EPCOS; Munich, Germany). Precision of the thermistors is ±0.2 °C. They had a distance of 7 cm to each other and the probe was installed with the upper two of the sensors placed in the pelagic water of the lake. Profiles were generally measured down to 0.91 m ($n = 13$). In some cases the sediments did not allow such a deep penetration of the probe, but the measurement depth was never less than 0.84 m ($n = 12$).

Measurements were conducted in an eight-day-period at the end of July 2012. In the eastern parts of the shoreline a section of 900 m was not covered by sediment temperature investigations because a broad belt of shoreline vegetation inhibited access and appropriate measurements.

The analytical solution of the heat transport equation results in the vertical Darcy velocity $q_z$ (m s$^{-1}$) (Bredehoeft and Papaopulos, 1965):

$$\frac{T(z)-T_0}{T_L-T_0}=\frac{\exp\left(\frac{q_z\rho_f c_f}{K_{fs}}z\right)-1}{\exp\left(\frac{q_z\rho_f c_f}{K_{fs}}L\right)-1} \tag{3}$$

where $L$ is the vertical extent of the domain where temperature changes due to LGD (m), $T(z)$ is the lake bed temperature (°C) at sediment depth $z$ (m), $\rho_f c_f$ is the volumetric heat capacity of the fluid (J m$^{-3}$ K$^{-1}$), $K_{fs}$ is thermal conductivity of the saturated sediment (J s$^{-1}$ m$^{-1}$ K$^{-1}$), $T_0$ is the temperature for $z = 0$ (i.e. surface water temperature, °C), and $T_L$ is the temperature for $z = L$ (i.e. groundwater temperature, °C). The vertical Darcy velocity $q_z$ is derived by minimizing the root mean squared error (RMSE) between the n measured temperatures of a profile and the related simulated temperatures (Schmidt et al., 2006):

$$\mathrm{RMSE}=\sqrt{\frac{1}{n}\sum_{j=1}^{n}\left[T_j-\left(\frac{\exp\left(\frac{q_z\rho_f c_f}{K_{fs}}z_j\right)-1}{\exp\left(\frac{q_z\rho_f c_f}{K_{fs}}L\right)-1}(T_L-T_0)+T_0\right)\right]^2} \tag{4}$$

Boundary conditions were set to lake water temperatures for $T_0$ and to groundwater temperature for $T_L$. Groundwater at the four near-shore sites (Fig. 1) showed depth-dependent temperature differences, ranging from 10.5 °C to 12.7 °C. Thus, in a first approach $T_L$ was set to 11 °C, representing the mean temperature measured in the ten wells. But for this case simulated temperature profiles did not show good fits to the measured profiles. It seemed that a value of 11 °C for $T_L$ was too low. Thus, $T_L$ was set to 13 °C, which seemed to be plausible since near-surface groundwater showed similar temperatures (12.7 °C in 2–4 m below surface, at site 4, Fig. 1A) and most LGD was expected to originate from near-surface groundwater and might thus be heated up to >11 °C during the summer season.

The value for $\rho_f c_f$ is $4.19 \times 10^{-6}$ J m$^{-3}$ K$^{-1}$ for water. According to Stonestrom and Constantz (2003) $K_{fs}$ was set to 2 J s$^{-1}$ m$^{-1}$ K$^{-1}$ for the predominantly sandy sediments of Lake Arendsee. Since the temperature probe was inserted only about 1 m into the sediment it never covered the whole thickness $L$ of the transition zone.

A range of different values for the transition zone $L$ was tested to identify the best fit of measured and simulated sediment temperatures. This revealed that at low values for the transition zone $L$ LGD increases with increasing $L$ while the RMSE of measured versus simulated temperatures decreased. This observation was independent of the temperature $T_L$ at the lower boundary (Fig. 3). $T_L$ was set to 13 °C which resulted in best fits in most cases (Fig. 3E). Due to the fact that the RMSE did not change at $L > 5$, $L$ was set to 5 m (Fig. 3C and D). Resulting values for $q_z$ were converted from discharge velocity (m s$^{-1}$) into daily LGD volume (l m$^{-2}$ d$^{-1}$).

### 2.6. Combination of hydraulic methods

Finally, we combined the results of the total annual volume of LGD and the LGD pattern to specify the amount of LGD for single shoreline sub-sections. Please note that from lake bed temperature derived LGD volumes only the maximum value of a transect was applied for further calculations. According to the numbers of lake bed temperature transects the shoreline was divided into 26 sub-sections by cutting the shoreline at each midpoint between two neighboring transects. The total annual volume of LGD based on groundwater recharge was split into 26 portions ($Q_{rech,i}$ in l yr$^{-1}$, in Eq. (5)) which considered the individual length $l_i$ of each shoreline sub-section. The ultimate amount of LGD discharging along a shoreline sub-section $i$ ($Q_i$ in l yr$^{-1}$) was calculated by the following equation:

$$Q_i = Q_{rech,i}\cdot\frac{q_{z,i}}{\overline{q_z}} \tag{5}$$

where $q_{z,i}$ is the maximum LGD rate (l m$^{-2}$ d$^{-1}$) derived from each four lake bed temperature profiles in shoreline section $i$ ($q_z$ in Eqs. (3) and (4)) and $\overline{q_z}$ is weighted arithmetic mean (l m$^{-2}$ d$^{-1}$) of all maximum lake bed temperature derived LGD rates ($q_{z,i}$) weighted by the individual length of the shoreline section $l_i$:

$$\overline{q_z}=\frac{\sum_{i=1}^{26}q_{z,i}\cdot l_i}{\sum_{i=1}^{26}l_i} \tag{6}$$

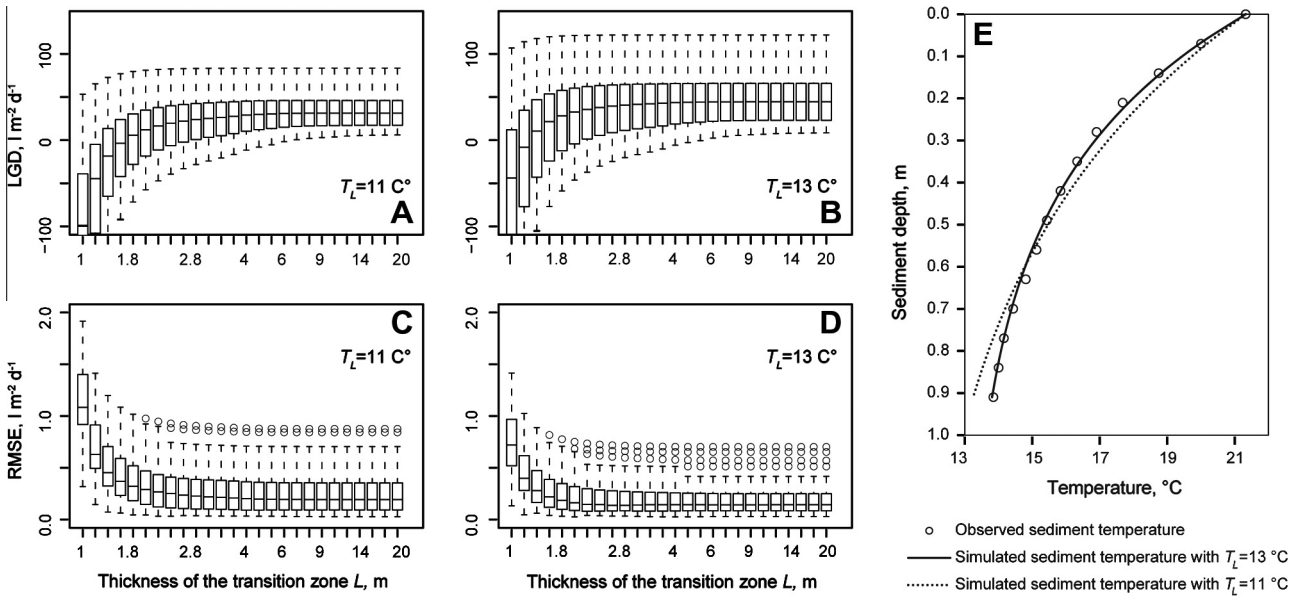


**Fig. 3.** Visualization of different parameters used in the heat transport equation (Eq. (3)). Boxplots of calculated lacustrine groundwater discharge (LGD) rates for $T_L$ = 11 °C (A) and $T_L$ = 13 °C (B) and root mean squared errors (RMSE) of measured versus simulated sediment temperatures for different values of the thickness of the transition zone $L$ (m) for $T_L$ = 11 °C (C) and $T_L$ = 13 °C (D). Note the irregular scaling of the $x$-axis in Fig.3A–D. Fig.3E shows an example for the results of temperature simulations for $T_L$ = 13 °C (continuous line) and $T_L$ = 11 °C (dotted line), based on measured temperatures (empty dots) and $L$ = 5 m. Simulations led to better fits and higher LGD for $T_L$ = 13 °C (RMSE: 0.09, LGD: 106 l m$^{-2}$ d$^{-1}$) compared to $T_L$ = 11 °C (RMSE: 0.37, LGD: 69 l m$^{-2}$ d$^{-1}$).

### 2.7. Phosphorus loads

To evaluate the necessity to determine LGD patterns with high spatial resolution we calculated three scenarios for groundwater-borne P loads to Lake Arendsee. Analysis of TP and SRP concentrations revealed that both are almost identical in this catchment. Thus, all scenarios are based on groundwater SRP concentrations measured at the four near-shore sites along the southern shoreline (Fig. 1A). At each site, either two or three groundwater observation wells are set up in different aquifer depths (Fig. 1B). Results of monthly or trimonthly measurements of SRP from April 2010 to December 2012 were available for each well. The four SRP concentrations used in the present study are means of these measurements, weighted by the thicknesses of geologic layers in which the wells are situated. Given that in many other case studies only a single groundwater observation well is available (if at all), Scenario 1 consists of four variants (1a to 1d), each based on the SRP concentration of one of the four sites for all 26 shoreline sub-sections. They correspond in their order to the order of the groundwater observation wells in Fig. 1A, with SRP concentrations of 0.09 mg l$^{-1}$ (1a), 0.16 mg l$^{-1}$ (1b), 1.21 mg l$^{-1}$ (1c), and 0.08 mg l$^{-1}$ (1d). P loads of each variant were calculated by multiplying the annual LGD volumes of each of the 26 shoreline sub-sections ($Q_i$ in Eq. (5)) by the corresponding SRP concentrations and summing up all 26 P loads. In Scenario 2, SRP concentrations all four sites were included simultaneously. Annual LGD volumes of the 26 sub-sections were multiplied by the mean SRP concentration of the closest measurement site. Scenario 3 considered the large heterogeneity of the near-shore groundwater concentrations at the four sites. The actual variation of the SRP concentrations in the near-shore wells might be log-normal distributed. Thus, for this scenario we assumed that SRP concentrations in the LGD of the 26 segments are as well log-normal distributed and that the concentrations found in the four groundwater observation wells characterize the arithmetic mean and the standard deviation of the log-normal distribution sufficiently well. With Microsoft Excel, we calculated 250 data sets, each consisting of 26 random SRP concentrations, which were log-normal distributed with the same arithmetic mean. We furthermore restricted the standard deviation to a 37% smaller value compared to the original standard deviation in order to avoid excessively high SRP concentrations. Each of the 26 SRP concentrations was assigned to one of the 26 shoreline sub-sections and multiplied by the corresponding annual LGD volume. Summing up all 26 values resulted in the total annual groundwater-borne P load of that data set. Thus, we finally ended up with 250 different groundwater-borne P loads in Scenario 3.

## 3. Results

### 3.1. Delineation of subsurface catchment

Hydraulic head data of 33 groundwater observation wells in the surrounding of Lake Arendsee facilitated the delineation of its subsurface catchment. The size and shape of the catchment were derived from the resulting hydraulic head contour lines. The catchment covered an area of 15.2 km$^2$ with a main expansion southeasterly of the lake (Fig. 4A). Dominating land use types were cropland and forest (35% each). The city of Arendsee, located directly at the southern shoreline, contributed with 14% and grassland with 18% to the area of the subsurface catchment (Table 1). Hydraulic head contour lines indicated a northern groundwater flow direction, with a steep hydraulic gradient in the western part of the catchment in the vicinity of Lake Arendsee that flattened in eastern direction (Fig. 4A).

### 3.2. Annual groundwater recharge and calculated drainage

Combinations of soil types and land uses in the subsurface catchment (Fig. 4A and B) resulted in 51 sub-areas for which groundwater recharge was individually calculated. Four land use types were included, as there are coniferous forest, cropland, grassland, and urban areas. Groundwater recharge rates were lowest in forested areas and highest in the urban area (Table 1). Croplands and grasslands differed in annual groundwater recharge rates (130 and 102 l m$^{-2}$ yr$^{-1}$, respectively), while the calculation of

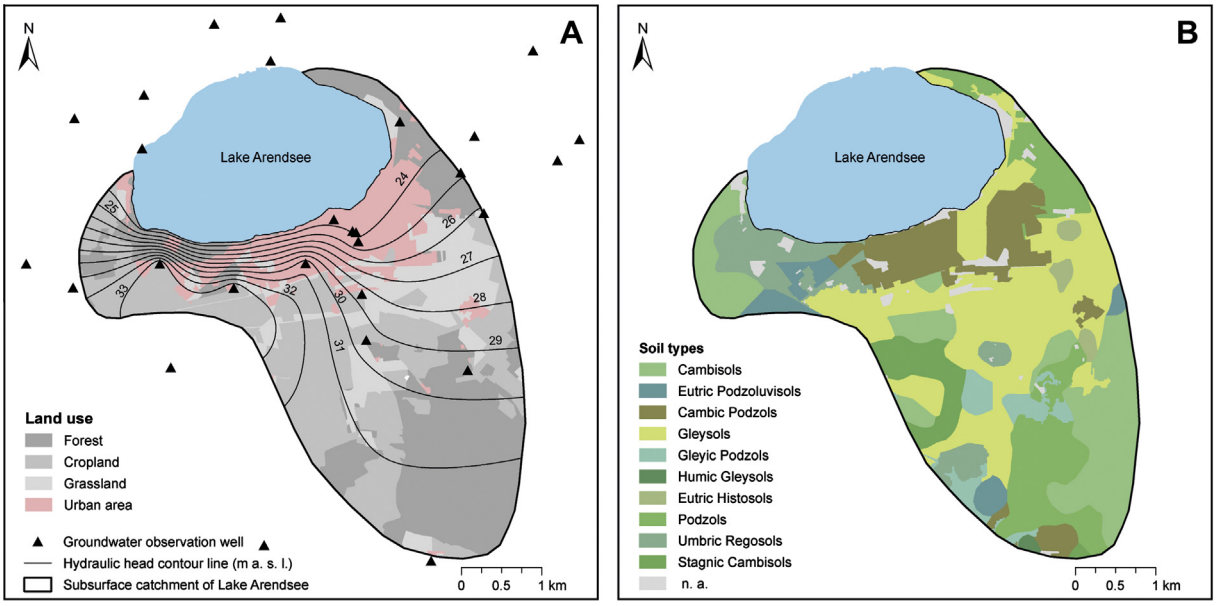


**Fig. 4.** Dominating land use types and hydraulic head contour lines (in m above sea level, narrow black lines) in the subsurface catchment of Lake Arendsee (bold black line), derived from hydraulic head measurements of observation wells (black triangles) in July 2012 (A). Soil types in the catchment of Lake Arendsee (B).

**Table 1**
Mean annual groundwater recharge rates ($l\,m^{-2}\,yr^{-1}$) of different land use types in the subsurface catchment of Lake Arendsee, calculated according to Glugla et al. (2003).

| | Area ($km^2$) | Groundwater recharge rate ($l\,m^{-2}\,yr^{-1}$) |
|---|---|---|
| Forest | 5.3 | 45 |
| Cropland | 5.3 | 130 |
| Grassland | 2.4 | 102 |
| Urban area | 2.2 | 189 |

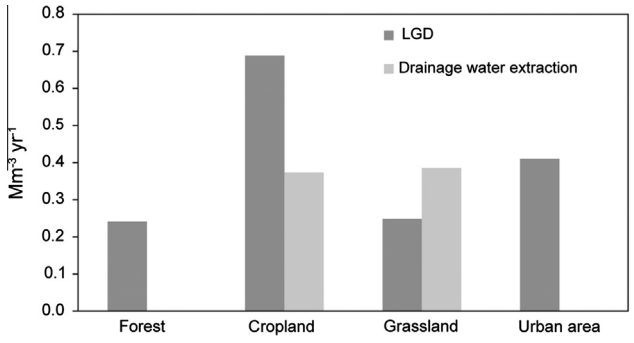


**Fig. 5.** Volumes of drainage water extracted from agricultural areas and land use dependent mean annual contribution to lacustrine groundwater discharge (LGD) ($Mm^3\,yr^{-1}$) derived from groundwater recharge calculations for the subsurface catchment according to Glugla et al. (2003).

drainage from drainage intensity classes resulted in similar values for absolute volumes (0.37 and 0.39 $Mm^3\,yr^{-1}$, respectively, Fig. 5). Taking the land use in the catchment into account, croplands contributed most to the LGD volume of Lake Arendsee (0.69 $Mm^3\,yr^{-1}$) followed by urban areas, mainly represented by the city of Arendsee (0.41 $Mm^3\,yr^{-1}$), grasslands and forests (0.25 and 0.24 $Mm^3\,yr^{-1}$, respectively) (Fig. 5). Accordingly, 1.27 $Mm^3$ entered Arendsee as total groundwater discharge per year (after having subtracted 0.32 $Mm^3$ for drinking water supply), while calculated drainage water extractions summed up to for 0.76 $Mm^3\,yr^{-1}$.

### 3.3. Measured drainage from agriculture

The one-year-period of drainage water measurements at the inflows of the drainage ditches to Lake Arendsee resulted in an overall drainage volume of 1.54 $Mm^3$. This exceeds the calculated mean annual drainage water extraction (0.76 $Mm^3$), and can be attributed to an above-average amount of precipitation during the year of that study. While mean annual precipitation sums up to 593 $l\,m^{-2}$ (1976–2007), this value was 746 $l\,m^{-2}$ in the measurement period from August 2010 until the end of July 2011. Measured drainage at the inflows to the lake accounted for 13.7% of precipitation, while a value of 8.4% of $\overline{P_{korr}}$ was calculated to discharge as drainage water from agricultural areas.

### 3.4. Spatial patterns of LGD

In many cases, the four measurements along one transect revealed a decrease of LGD with increasing distance to the shoreline. This decline occurred independently of flux intensities although sites with generally high LGD rates still showed high rates at large distances to the shoreline (Fig. 6) while sites with less intense LGD often did not reveal any LGD at these distances any more. We found maximum LGD rates in the central reach of the southern shoreline while in eastern and western directions, LGD was generally lower (Fig. 7). Also within the central part of the southern shoreline variation of LGD rates occurred: The maximum LGD rate was 122 $l\,m^{-2}\,d^{-1}$, while adjacent LGD rates in this section varied between 60 and 108 $l\,m^{-2}\,d^{-1}$. In western direction LGD rates decreased with one exception in a little bay at the south-western shoreline where LGD was much higher than at neighboring sites. A slight increase of LGD is also found along the eastern shoreline, although the subsurface catchment had a small extension in that area.

### 3.5. Shoreline sub-section LGD amounts

The 26 shoreline sub-sections had a mean length of 196 m, with a maximum of 245 m and a minimum of 113 m. This results from different distances between single transects of lake bed temperature profiles due to restricted accessibility of the shoreline in some

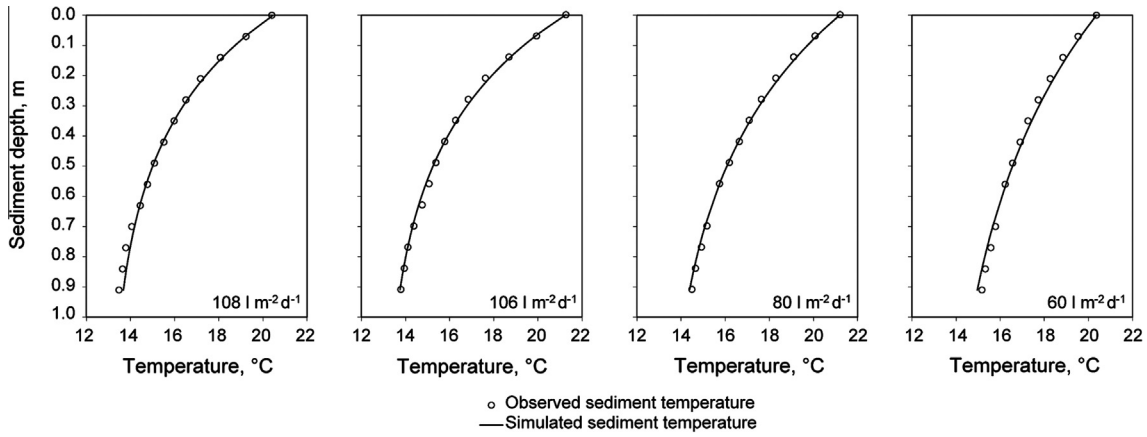


**Fig. 6.** Profiles of lake bed temperatures and resulting LGD rates in different distances to shoreline (0.5, 1.0, 2.0, and 4.0 m from left to right).

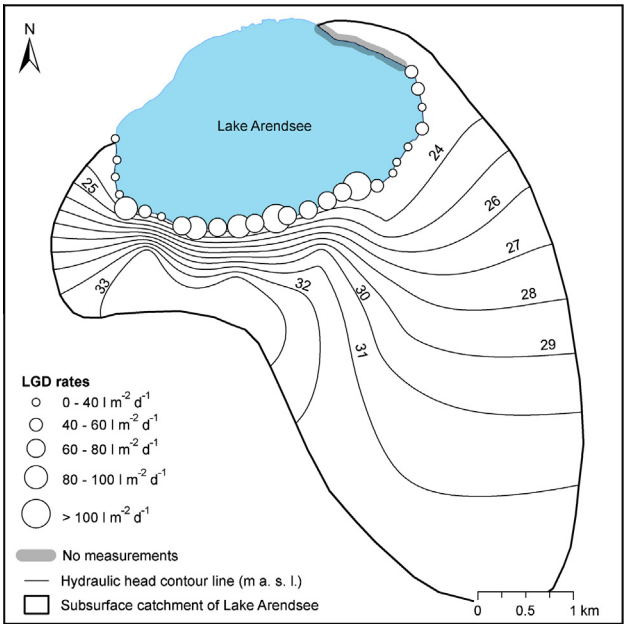


**Fig. 7.** Maximum LGD rates ($l\,m^{-2}\,d^{-1}$) derived from transects of four sediment temperature depth profiles at each observation site in Lake Arendsee. A 900 m-reach along the north-eastern shoreline (shaded in grey) was not accessible and thus excluded from sediment temperature measurements. Narrow black lines represent hydraulic head contour lines (in m above sea level) in the subsurface catchment (bold black line).

cases. Main LGD occurred within a section of 2.19 km at the southern shoreline, where an amount 0.69 $Mm^3\,yr^{-1}$ of LGD is calculated. This equaled an amount of 54% of the total LGD entering

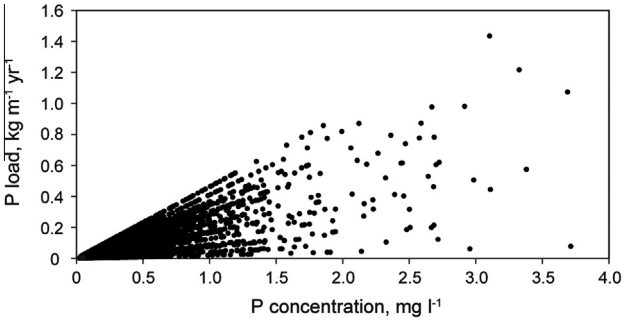


**Fig. 8.** Random P concentrations (mg SRP $l^{-1}$) for shoreline sub-sections and resulting sub-sectional groundwater P loads calculated for Scenario 3. For comparability P loads are normalized to P entering the lake along one meter of shoreline during a one-year-period (kg P $m^{-1}\,yr^{-1}$).

the lake along 36% of the shoreline bordering on the subsurface catchment and 24% of the total shoreline. Results normalized to 200 m shoreline sub-sections ranged between 0.004 and 0.093 $Mm^3\,yr^{-1}$.

### 3.6. Groundwater-borne phosphorus loads

Based on the results for annual LGD in sub-sections of the shoreline, groundwater-borne P loads were calculated for three different scenarios. P loads in the scenario-variants 1a, b and d (based on the same single groundwater SRP concentration for all shoreline sub-sections), range between 81 and 170 kg P $yr^{-1}$. For variant 1c the calculated P load is about ten times higher (1307 kg P $yr^{-1}$, Table 2). Scenario 2, in which the SRP concentrations of the four observation sites along the shoreline are

**Table 2**
Means and coefficients of variance (CV) for the three different scenarios used for P load calculations. Results for sub-sectionial P loads are normalized to a P load entering the lake along one meter of shoreline per year (kg $m^{-1}\,yr^{-1}$). Concentrations used for Scenarios 1a to 1d are mean SRP concentrations of one of the four near-shore groundwater (GW) observation sites that are also used as SRP concentrations in Scenario 2 but are allocated to different sub-sections in that scenario. Scenario 3 uses random distributions of SRP concentrations based on the arithmetic mean and standard deviation of the four measured SRP concentrations.

| | Scenario 1a (0.09 mg $l^{-1}$) | Scenario 1b (0.16 mg $l^{-1}$) | Scenario 1c (1.21 mg $l^{-1}$) | Scenario 1d (0.08 mg $l^{-1}$) | Scenario 2 | Scenario 3 |
|---|---|---|---|---|---|---|
| Corresponding GW observation site in Fig. 1 | 1 | 2 | 3 | 4 | 1–4 | – |
| *n* (different P concentrations of LGD) | 1 | 1 | 1 | 1 | 4 | 26 · 250 |
| *n* (different P loads of shoreline sub-sections) | 26 | 26 | 26 | 26 | 26 | 26 · 250 |
| Mean P load of shoreline sub-sections (kg P $m^{-1}\,yr^{-1}$) | 0.02 | 0.033 | 0.255 | 0.016 | 0.081 | 0.079 |
| CV | 0.581 | 0.581 | 0.581 | 0.581 | 1.650 | 1.222 |
| Total P load (kg P $yr^{-1}$) | 102 | 170 | 1307 | 81 | 425 | 212–891 |

considered, results in an annual P load of 425 kg P $yr^{-1}$. Scenario 3 was calculated for 250 variants resulting in total annual P loads of 212–891 kg P $yr^{-1}$. Mean P loads of shoreline segments (normalized to P load discharging along one meter of shoreline per year, kg $m^{-1}$ $yr^{-1}$), and mean total P load (not shown) are similar to those of Scenario 2 since the data set was created based on this similarity. The maximum out of 26 · 250 SRP concentrations was 3.71 mg $l^{-1}$. This seems to be quite high but measurements of near-shore groundwater close to the surface (unpublished data) revealed SRP concentrations of >4 mg $l^{-1}$. Thus, a value of 3.71 mg $l^{-1}$ is adequate to represent maximum groundwater SRP concentrations. Coefficients of variance were the same for all variants in Scenario 1 since LGD was the only variation between sub-sections while concentrations were the same in all of them. In contrast, coefficients of variance were clearly increased in Scenarios 2 and 3 to a value of >1.

The impact of LGD on P loads is demonstrated by the comparison of P concentrations and resulting P loads in Scenario 3 (Fig. 8). It becomes obvious that P loads can be low although the corresponding P concentration is high and vice versa. For example, the two maximum SRP concentrations generated in Scenario 3 (3.69 and 3.71 mg $l^{-1}$) resulted in strongly differing sub-section P loads (1.07 and 0.078 kg $m^{-1}$ $yr^{-1}$, respectively) because of different LGD rates.

## 4. Discussion

### 4.1. Groundwater recharge

By calculating groundwater recharge according to Glugla et al. (2003) based on the available data on land use and soil parameters, the estimated groundwater recharge rates are reliable with a high spatial resolution. Although the method is based on data for Germany, comparable approaches should be available for any region of interest, at least in humid climates. However, problems may arise in many regions due to a lack of data concerning artificial reduction of groundwater recharge. For example, as mentioned in the result section, an amount of 0.32 $Mm^3$ of groundwater is annually extracted from the aquifer for drinking water supply. Another ubiquitous reduction of groundwater recharge is the drainage of agricultural areas for melioration. In the present study, 35% of the total discharge ($\overline{R}$ in Eq. (2)) from croplands was calculated to be drainage water (section 2.3), while this value even exceeds 60% below grasslands (Fig. 5). Mathematically, these drainage efforts lead to a reduction of the actual groundwater recharge by 32% compared to original (natural) conditions. This highlights the enormous impact of drainage for water balances of mainly agricultural catchments. Nevertheless, quantitative information on drainage of agricultural plains might be hardly available and of limited reliability. Depending on the context, this might restrict the validity of groundwater recharge calculations. In the present case, fortunately, data on drainage intensities were available and additionally confirmed by actually measured drainage volumes. Measured results were even higher than calculated, which underlines the importance of drainage extractions for actual groundwater recharge in agricultural areas. However, the drainage portions of 13.7% (measured) and 8.4% (calculated) of $\overline{P_{korr}}$ confirm the general results of the groundwater recharge calculations, since the reference period experienced an amount of precipitation that was 25% larger than the mean annual precipitation. This probably led to a corresponding increase of drainage.

Although the urban area covers a relatively small portion of the subsurface catchment (Table 1) it contributes the second largest portion to the total LGD volume (Fig. 5). Considered as grassland without drainage water extraction, groundwater recharge exceeds rates calculated for agricultural grasslands by far although 30% of the urban area is sealed and thus inactive regarding groundwater recharge.

### 4.2. LGD patterns and P loads

A total of 33 groundwater observation wells is a fairly good basis for an overview of the hydraulic characteristics of a subsurface catchment of this size. With these data, it is possible to determine the spatial extent of the subsurface catchment with a high degree of accuracy. Furthermore, the hydraulic head contour lines that are interpolated from the groundwater head data reveal general groundwater flow directions that confirmed the assumption of main LGD in the southern part of the shoreline (Fig. 7). However, they do not represent actual small scale heterogeneity of LGD at the shoreline at all. Changes in geologic composition of the aquifer material close to the lake are expected to cause substantial heterogeneity in LGD. For example, coarse material embedded in less permeable sediments may cause preferential flow paths, resulting in significantly higher, but spatially isolated LGD rates (Krabbenhoft and Anderson, 1986). This might be the reason for the above mentioned single site in the south-western part of the shoreline showing a relatively high LGD rate. Another reason for increased LGD at that site might be its location in an embayment. LGD in bays is commonly larger since flow paths originating from different directions are focused in these locations (Cherkauer and McKereghan, 1991). Measured LGD rates at the eastern shore (public sand beach) are surprisingly high and in no agreement with the size of the catchment or the surface topography. We assume that the high rates are caused by lake water recirculation. Sea water recirculation is well known for submarine groundwater discharge (SGD; Taniguchi et al., 2002). Due to the intense wave activity at the eastern shore lake water might recirculate at this shore. However, to the best of our knowledge such a process has never been reported for lacustrine settings.

Anthropogenic alteration of the shoreline might additionally affect the LGD patterns. For example, shoreline stabilization might inhibit LGD. Vegetation growth along the shoreline might cause a decrease of LGD since vegetation usually results in an accumulation of fine sediments, thus a lower hydraulic conductivity and emersed vegetation might even result in a transpiration of subsurface water prior to its discharge into the lake.

Compared to what was expected based on hydraulic head contour lines, sediment temperature profiles revealed that the shoreline section of main LGD is shifted eastwards by several hundreds of meters. Furthermore, using heat as a tracer showed an intense variety of LGD rates on the medium-scale. This variety occurred even within the limited section in the south of the lake where LGD was largest (60–122 l $m^{-2}$ $d^{-1}$). It should be noted that studies on small-scale heterogeneity of groundwater–surface water interaction revealed a spatial variability that is beyond the scale of the present study (e.g. Kishel and Gerla, 2002). But these small-scale heterogeneities are likely superimposed by the medium-scale local groundwater flow regime. A higher measurement resolution of lake bed temperatures would have certainly resulted in a finer pattern of LGD rates in the present study. However, it is doubtful whether that increase of accuracy is worth the substantial effort of further field measurements. By upscaling the results to shoreline sub-sections with a length of approximately 200 m we generally improved the qualitative and quantitative description of LGD volumes and groundwater-borne P loads to a large extent compared to integrating approaches. For the determination of P loads the knowledge of both, spatial patterns of LGD and SRP concentrations is essential. This is illustrated by the three different scenarios of P load determination (Table 2). In Scenario 1, P loads of all 26 shoreline sections are based on

the SRP concentration of a single groundwater observation site. Consequently, P loads vary in the same range as sub-sectional LGD volumes do and the section of intense P loads is consistent with major LGD all along the southern shoreline (Fig. 7). In these cases, the spatial pattern of LGD controls the P input to the lake. With heterogeneous SRP concentrations in the discharging groundwater a stronger variation in sub-sectional P loads occurs. In the case of Scenario 2, the actually measured SRP concentrations at four different sites imply a main P load in a relatively short section at the south-southeastern shoreline around Site 3 in Fig. 1. Both, LGD and the SRP concentration are high in that area. In other sub-sections P loads are low although LGD is relatively high. This heterogeneity of P loads induced by SRP concentration is also represented by a much higher coefficient of variation (Table 2). However, P loads in Scenario 3 range from 212 to 891 kg $yr^{-1}$ which demonstrates the influence of spatial LGD patterns on groundwater-borne nutrient loads, especially in combination with heterogeneous nutrient concentrations.

If high variability of nutrient concentrations occur or are expected, spatial patterns of LGD should be carefully considered: Scenario 2 results in an overall P load of 425 kg $yr^{-1}$. Without considering the results of lake bed temperature measurements as a weighting factor for spatial LGD patterns, the calculation of the P load yielded only 327 kg $yr^{-1}$. This deviation of approximately 25% might still be acceptable compared to uncertainties of other input paths in the P balance of the lake. However, the relatively good agreement of the calculation with and without weighting factor is based on the fact that that the zones of major LGD volumes and highest groundwater SRP concentrations coincidence in the present case study. As illustrated by Scenario 3 total P loads can broadly vary because of this dependency of P loads on both LGD volumes and SRP concentrations (Table 2).

Furthermore, not only actual values for nutrient loads but also the localization of their sources might be of interest. LGD patterns help to find hot spots or sections of intense nutrient exfiltration along the shoreline. Tracking back groundwater flow directions from there might help to identify contaminated sites. Another reason for taking LGD patterns into account is the planning of effective *in situ*-restoration measures.

However, uncertainties in LGD pattern identification might arise from improper estimation of boundary conditions in the procedure of solving the heat transport equation (Eqs. (3) and (4)). As described above, groundwater temperatures might vary in time, as well as in horizontal and lateral space. The approach is designed for assumed 1-D vertical fluxes only, although actual groundwater flow lines would describe a mixture of both, vertical and lateral fluxes (Rosenberry and LaBaugh, 2008). In the present case relatively high temperatures for the lower boundary condition $L$ indicate a rather lateral inflow of near-surface (and thus warmer) groundwater. This issue is especially discussed by Ferguson and Bense (2011). Further uncertainty might be introduced by the term of thermal conductivity ($K_{fs}$). This value is commonly estimated from literature, since its empirical determination is elaborate, especially under heterogeneous sediment conditions. In general, values for $K_{fs}$ in saturated sediments vary only little (between 1.4 J $s^{-1}$ $m^{-1}$ $K^{-1}$ for clayey and 2.2 J $s^{-1}$ $m^{-1}$ $K^{-1}$ for sandy sediments, as shown in Stonestrom and Constantz, 2003). Nevertheless, this might be an important factor if absolute LGD rates are required, since resulting exfiltration rates change by the degree of changes in $K_{fs}$. If, as in this study, resulting LGD rates are not processed as absolute results, but used as a measure for exfiltration intensity, this issue is reduced. Many critiques for using heat as a tracer for groundwater–surface water interactions deal with different aspects of diverse boundary conditions (Ferguson and Bense, 2011; Kalbus et al., 2006; Schmidt et al., 2007).

## 5. Conclusion

Calculating groundwater recharge in the catchment to determine the groundwater component in the water balance of a lake is no new approach. However, special care is required when the water balance serves as a prerequisite of the nutrient budget. As shown in the present study, it might be insufficient to multiply the total annual LGD volume with the mean groundwater nutrient concentration to determine the absolute nutrient load. Spatial heterogeneities of groundwater quality and LGD need to be considered carefully for reliable quantifications of groundwater-borne nutrient loads. Unfortunately, an adequate number of groundwater observation wells or other possibilities to capture heterogeneities in nutrient concentrations are often not available. Thus, the nutrient concentrations finally applied to the setup of the budget underlie some uncertainty. If the total LGD volume is imprecise, a factor of uncertainty is imposed on the nutrient budget. If additionally fine-scaled spatial patterns of LGD are unconsidered, further uncertainty is introduced. Accordingly, the groundwater impact on the lakés ecosystem might be severely over- or underestimated. As a consequence, this might even lead to a failure of restoration efforts, if measures are based on insufficient nutrient budgets.

The presented approach of combining total groundwater recharge volumes and LGD patterns drastically reduces the uncertainty of the groundwater component in the nutrient balance of Lake Arendsee. Uncertainties of temperature based LGD rates are minimized by reducing their role to a weighting factor (instead of using absolute values) for groundwater recharge calculations. Different scenarios proved the great importance of spatial LGD patterns for groundwater-borne nutrient loads.

## Acknowledgements

We thank Franziska Pöschke and Sebastian Rudnick as well as Thomas Mehner for helpful discussions in the early stage of the manuscript. For field data sampling we thank Mathias Solzbacher and Guido Taborski. This research was funded by the State Agency for Flood Protection and Water Management Saxony-Anhalt (LHW).

## References

Anderson, M.P., 2005. Heat as a ground water tracer. Ground Water 43 (6), 951–968.
Bagrov, N.A., 1953. O srednem mnogoletnem ísparenii s poverchnosti suši (On the mean long-term evaporation rates from the continental surface, in Russian). Meteorol. Gidrologia 10, 10–20.
Bredehoeft, J.D., Papaopulos, I.S., 1965. Rates of vertical groundwater movement estimated from the Earth's thermal profile. Water Resour. Res. 1 (2), 325–328.
Bremer, J.E., Harter, T., 2012. Domestic wells have high probability of pumping septic tank leachate. Hydrol. Earth Syst. Sci. 16 (8), 2453–2467.
BÜK 1000, 1998. Soil Map of the Federal Republic of Germany 1:1,000,000; digital map. Federal Institute for Geosciences and Natural Resources (Ed.), first ed., Berlin.
Cherkauer, D.S., McKereghan, P.F., 1991. Groundwater discharge to lakes – focusing in embayments. Ground Water 29 (1), 72–80.
Constantz, J., 2008. Heat as a tracer to determine streambed water exchanges. Water Resour. Res. 44.
Ferguson, G., Bense, V., 2011. Uncertainty in 1D heat-flow analysis to estimate groundwater discharge to a stream. Ground Water 49 (3), 336–347.
Gelbrecht, J., Lengsfeld, H., Pöthig, R., Opitz, D., 2005. Temporal and spatial variation of phosphorus input, retention and loss in a small catchment of NE Germany. J. Hydrol. 304 (1–4), 151–165.
Glugla, G., Jankiewicz, P., Rachimow, C., Lojek, K., Richter, K., Fürtig, G., Krahe, P., 2003. Hydrological balance model to determine regional annual evaporation losses and runoff rates under different climatic conditions (Wasserhaushaltsverfahren zur Berechnung vieljähriger Mittelwerte der tatsächlichen Verdunstung und des Gesamtabflusses, in German). Federal Institute of Hydrology, BfG-Report 1342, Koblenz, 118p.
Hupfer, M., Lewandowski, J., 2005. Retention and early diagenetic transformation of phosphorus in Lake Arendsee (Germany) – consequences for management strategies. Arch. Hydrobiol. 164 (2), 143–167.
Kalbus, E., Reinstorf, F., Schirmer, M., 2006. Measuring methods for groundwater – surface water interactions: a review. Hydrol. Earth Syst. Sci. 10 (6), 873–887.

Katz, B.G., Eberts, S.M., Kauffman, L.J., 2011. Using Cl/Br ratios and other indicators to assess potential impacts on groundwater quality from septic systems: a review and examples from principal aquifers in the United States. J. Hydrol. 397 (3–4), 151–166.
Kishel, H.F., Gerla, P.J., 2002. Characteristics of preferential flow and groundwater discharge to Shingobee Lake, Minnesota, USA. Hydrol. Process. 16 (10), 1921–1934.
Krabbenhoft, D.P., Anderson, M.P., 1986. Use of a numerical groundwater-flow model for hypothesis-testing. Ground Water 24 (1), 49–55.
McBride, M.S., Pfannkuch, H.O., 1975. Distribution of seepage within lakebeds. J. Res. Geol. Survey 3 (5), 505–512.
Meyboom, P., 1967. Mass-transfer studies to determine the groundwater regime of permanent lakes in hummocky moraine of Western Canada. J. Hydrol. 5, 117–142.
Moss, B., 2012. Cogs in the endless machine: Lakes, climate change and nutrient cycles: a review. Sci. Total Environ. 434, 130–142.
Ptacek, C.J., 1998. Geochemistry of a septic-system plume in a coastal barrier bar, Point Pelee, Ontario, Canada. J. Contam. Hydrol. 33 (3–4), 293–312.
Robertson, W.D., 2008. Irreversible phosphorus sorption in septic system plumes? Ground Water 46 (1), 51–60.
Rosenberry, D.O., LaBaugh, J.W., 2008. Field Techniques for Estimating Water Fluxes between Surface Water and Ground Water. US Geological Survey Techniques and Methods 4-D2, Reston, 128p.
Scanlon, B., Healy, R., Cook, P., 2002. Choosing appropriate techniques for quantifying groundwater recharge. Hydrogeol. J. 10 (1), 18–39.
Schmidt, C., Bayer-Raich, M., Schirmer, M., 2006. Characterization of spatial heterogeneity of groundwater–stream water interactions using multiple depth streambed temperature measurements at the reach scale. Hydrol. Earth Syst. Sci. 10 (6), 849–859.
Schmidt, C., Conant Jr., B., Bayer-Raich, M., Schirmer, M., 2007. Evaluation and field-scale application of an analytical method to quantify groundwater discharge using mapped streambed temperatures. J. Hydrol. 347 (3–4), 292–307.
Stonestrom, D., Constantz, J., 2003. Heat as a Tool for Studying the Movement of Ground Water Near Streams. US Department of the Interior Circular 1260, Reston, 105p.
Taniguchi, M., Burnett, W.C., Cable, J.E., Turner, J.V., 2002. Investigation of submarine groundwater discharge. Hydrol. Process. 16 (11), 2115–2129.
Winter, T.C., 1999. Relation of streams, lakes, and wetlands to groundwater flow systems. Hydrogeol. J. 7 (1), 28–45.